J Mol Model (2014) 20:2459
DOI 10.1007/s00894-014-2459-2

ORIGINAL PAPER

Structural characteristics of liquid nitromethane at the nanoscale confinement in carbon nanotubes

Yingzhe Liu · Weipeng Lai · Tao Yu · Zhongxue Ge · Ying Kang

Received: 24 March 2014 / Accepted: 2 September 2014 / Published online: 18 September 2014

Abstract The stability of energetic materials confined in the carbon nanotubes can be improved at ambient pressure and room temperature, leading to potential energy storage and controlled energy release. However, the microscopic structure of confined energetic materials and the role played by the confinement size are still fragmentary. In this study, molecular dynamics simulations have been performed to explore the structural characteristics of liquid nitromethane (NM), one of the simplest energetic materials, confined in a series of armchair single-walled carbon nanotubes (SWNTs) changing from (5,5) to (16,16) at ambient conditions. The simulation results show that the size-dependent ordered structures of NM with preferred orientations are formed inside the tubular cavities driven by the van der Waals attractions between NM and SWNT together with the dipole-dipole interactions of NM, giving rise to a higher local mass density than that of bulk NM. The NM dipoles prefer to align parallel along the SWNT axis in an end-to-end fashion inside all the nanotubes except the (7,7) SWNT where a unique staggered orientation of NM dipoles perpendicular to the SWNT axis is observed. As the SWNT radius increases, the structural arrangements and dipole orientations of NM become disordered as a result of the weakening of van der Waals interactions between NM and SWNT.

Keywords Dipole-dipole interactions · Energetic materials · Molecular dynamics simulations · Ordered nanostructures

Introduction

Developing new energetic materials with excellent power and safety is a great challenge because of an essential contradiction between the power and safety, i.e., high power generally couples with low safety. In recent years, research on increasing the energy density has made tremendous advancement and a few high-energy-density materials (HEDMs) have been discovered, such as polymeric nitrogen [1]. The energy density of polymeric nitrogen linked by the single bond has been predicted to be at least three times higher than that of the most powerful energetic materials known today [2]. However, the stability of these HEDMs, an important issue of safety, is still a big bottleneck, which may greatly impede the fabrication of HEDMs at ambient pressure and room temperature, energy storage, and controlled energy release.

Carbon nanotubes (CNTs) have been the object of an increased interest on account of their striking structures, as well as remarkable properties ranging from high thermal and electrical, great mechanical strength, to excellent chemical stability [3]. Recent studies have shown that confinement of some molecules into the CNT cavity can improve stability, give rise to unique intermolecular arrangements, and bring about lowering of activation barriers for certain reactions [4]. Subsequently, the effect of CNT confinement on the stability of energetic materials was probed theoretically at first due to the experiment difficulties as well as the time and money cost on synthesis of these systems. For example, Abou-Rachid and co-workers reported that the polymeric nitrogen confined in a CNT or a graphene matrix can be stable at ambient pressure and room temperature, and the stability is governed by the charge transfer between polymeric nitrogen and carbon nanostructures [5–7]. The same

Electronic supplementary material The online version of this article (doi:10.1007/s00894-014-2459-2) contains supplementary material, which is available to authorized users.

Y. Liu (✉) · W. Lai · T. Yu · Z. Ge · Y. Kang
Xi'an Modern Chemistry Research Institute, Xi'an 710065, People's Republic of China
e-mail: liuyz_204@163.com

T. Yu
School of Materials Science and Engineering, Fuzhou University, Fuzhou 350108, People's Republic of China

interaction mechanism also leads to the stability of polymeric nitrogen and polynitrogen clusters confined in the CNT bundle [8] and fullerene [9] at ambient conditions, respectively. In addition to HDEMs, the explosives, such as FOX-7 (1,1-diamino-2,2-dinitroethylene), RDX (hexahydro-1,3,5-trinitrostriazine), HMX (octahydro-1,3,5,7-tetranitro-1,3,5,7-tetrazocine), etc., can be stabilized when encapsulated inside a CNT or graphene layers, driven by the synthetic interactions of intermolecular H-bonding, charge transfer, and dispersion interactions between the energetic molecules and carbon nanostructures [10]. However, the structure features of confined energetic molecules involving intermolecular interactions are still fragmentary, in particular the influence of confinement size.

Nitromethane (NM) is one of the simplest nitro compounds that are of great interest to the high explosives community. On account of its relatively small size and availability of extensive experimental data, NM has been intensively used as a prototype system in theoretical studies of energetic materials, ranging from structure properties [11–17], melting and crystallization [18, 19], to thermal decomposition [20–27]. Although NM has a simple structure, its thermal decomposition mechanism is very complex because many species and elementary reactions will occur in the process of decomposition. At certain nanoscale confinement, the orientation and arrangement of confined NM would be different from that of bulk NM, which may lead to a different or controlled decomposition mechanism. The quantum mechanics study has shown that the structural rearrangement and thermal decomposition reactions of NM is promoted at the confinement of a (5,5) CNT [22]. Therefore, the investigations on the structural characteristics of confined NM from the theoretical view will help us understand the stabilization, confined decomposition pathway, and controlled energy release of nanostructured energetic materials.

In the present contribution, all-atom molecular dynamics (MD) simulations have been performed to explore the structural characteristics of the liquid NM confined in a single-walled carbon nanotube (SWNT) at ambient conditions. To further investigate the effect of confinement size on the orientation and arrangement of NM molecules, a series of SWNTs with different radius were examined.

Methods

Molecular models The NM molecule has two different conformers, i.e., *eclipsed* and *staggered* form (see Fig. 1a, b), and the energy barrier of transform between them is less than 0.01 kcal mol^{-1} in the gas phase, suggesting that the NO_2 group can rotate around the C–N bond almost freely [16]. Hence, only the staggered form of isolated NM molecule was built and optimized at first. The liquid NM was then modeled by constructing a simulation box that is composed of 1728 optimized NM molecules. Finally, a 10 ns equilibrium simulation of the liquid NM was performed under the temperature of 300 K and the pressure of 1 bar. The simulation results show that *eclipsed* and *staggered* conformations of NM occur equally (see Fig. S1 in Supporting information). In addition, the average mass density of liquid NM obtained from the simulation trajectory is 1.111 g/cm^3, which is close to the experimental value of 1.137 g/cm^3 at 293 K [28].

SWNT To model the nanoscale confinement, undecorated and ideal SWNTs of the armchair type with (*n*,*n*) indices were employed. The SWNT can be regarded as a tube rolled up by the single layer of graphite shell, and thus the corresponding radius of armchair SWNT can be calculated on the basis of the following equation [29]:

$$r_0 = 3na/2\pi, \tag{1}$$

where r_0 is the SWNT radius, n is the index for the armchair SWNTs, and a=0.142 nm is the length of C–C bond. To probe the influence of confinement size on the structural feature of confined NM, a series of (*n*,*n*) SWNTs with n ranging from 5 to 16, corresponding to the SWNT radius of 0.339 ~ 1.085 nm (see Table 1), were considered. The lengths of all the SWNTs were chosen to be about 3.0 nm.

[a] The (*n*, *n*) entries represent the indices of armchair SWNT; r_0 is the radius of SWNT; N_C is the number of carbon atoms of SWNT; N_{NM} is the number of NM molecules; N_{in} is the average number of NM confined in the middle 2.0 nm of SWNT.

Initially, SWNT was immersed into the NM solvents and placed at the center of the simulation box, with the SWNT axis along the z direction (see Fig. 1c). Then the NM molecules within 0.24 nm of SWNT were removed to avoid poor atomic contacts and ensure a spontaneous entrance of NM into the interior of nanotubes. Herein, the positions of all SWNT atoms were restrained by means of a weak harmonic potential of 1.0 kcal mol^{-1}. To eliminate possible edge effects, only the region of 2.0 nm within the middle of SWNT was analyzed.

Molecular dynamics simulations The CHARMM36 general force field [30] was employed to describe the NM molecules. All the SWNT atoms were described by means of the sp^2 aromatic carbon parameters of the CHARMM27 force filed [31] devoid of a net atomic charge. The form of the CHARMM potential energy functions used to calculate the potential energy, $V(r)$, is given in the following equation:

$$\begin{aligned} V(r) = & \sum_{bonds} K_b(b-b_0)^2 + \sum_{angles} K_\theta(\theta-\theta_0)^2 \\ & + \sum_{dihedras} K_\phi(1+\cos(n\phi-\delta)) \\ & + \sum_{improper} K\varphi(\varphi-\varphi_0)^2 + \sum_{Urey-Bradtey} K_{UB}\left(r_{1,3}-r_{1,3:0}\right)^2, \\ & + \sum_{nonbonded} \varepsilon_{ij}\left[\left(\frac{R_{\min,ij}}{r_{ij}}\right)^{12} - 2\left(\frac{R_{\min,ij}}{r_{ij}}\right)^{6}\right] + \frac{q_i q_j}{4\pi D r_{ij}} \end{aligned} \tag{2}$$

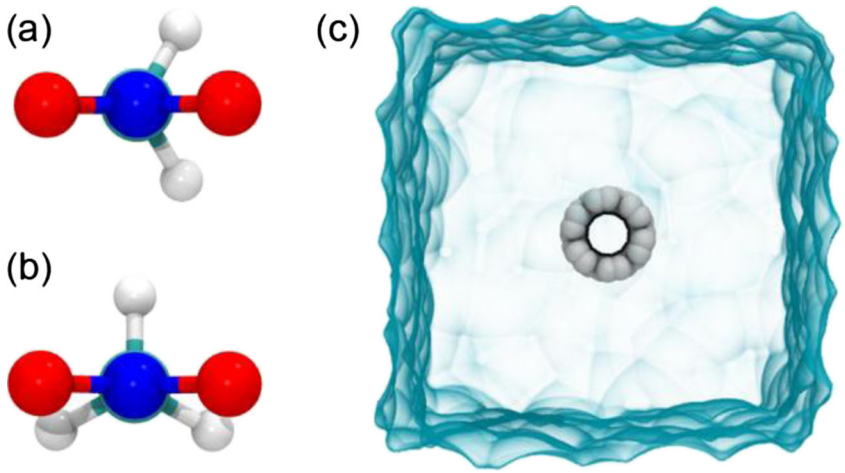

Fig. 1 The structure of (**a**) *eclipsed* NM, (**b**) *staggered* NM, and (**c**) a (6,6) SWNT immersed in NM solvent for the MD simulation

where r represents the Cartesian coordinates of the system; b_0, θ_0, φ_0, and $r_{1,3;0}$ are the bond, angle, improper, and Urey-Bradley equilibrium terms, respectively, n and δ are the dihedral multiplicity and phase and the K's are the respective force constants, ε_{ij}, $R_{\min,ij}$, and r_{ij} are the Lennard-Jones well depth, the minimum interaction radius, and the distance between atom i and j, respectively, q_i and q_j is the partial atomic charge of atom i and j that is obtained from the quantum mechanics calculations, D is the dielectric constant.

All the MD simulations were performed using the program NAMD2.9 [32] in the isobaric-isothermal ensemble with periodic boundary conditions applied in three directions of Cartesian space. The temperature and the pressure were maintained at 300 K and 1 bar, respectively, employing Langevin dynamics and Langvein piston pressure control [33]. The equations of motion were integrated using the multiple time-step Verlet r-RESPA algorithm [34] with time steps of 2 and 4 fs for short- and long-range interactions, respectively. Covalent bonds involving hydrogen atoms were constrained to their equilibrium lengths by means of the SHAKE/RATTLE algorithms [35, 36]. A smoothed of 1.2 nm spherical cutoff was used to truncate van der Waals interactions, and long-range electrostatic forces were evaluated employing the particle mesh Ewald approach [37].

Each molecular system before production simulation underwent 5000 steps of energy minimization, 50 ps of heating process from 0 to 300 K at the fixed volume by reassigning velocities, followed by 50 ps of equilibration at 300 K and 1 bar. Then, the production simulation was performed for 10 ns. To determine whether the molecular systems are sufficiently equilibrated, the number of the NM molecules confined in the tubular cavity as a function of simulation time was monitored. As displayed in Fig. S2, the number of confined NM molecules during the simulation trajectory of the last 5 ns fluctuates steadily in all the systems, suggesting that the time scale of 10 ns is suitable for the investigation on the structural characteristics of confined NM. Accordingly, the simulation trajectory of the last 5 ns was chosen for the analysis. Analysis and visualization of simulation trajectories were performed with the VMD package [38].

Table 1 Detail of NM-SWNT systems for molecular dynamics simulation

(n, n)	r_0/nm	N_C	N_{NM}	N_{in}
(5, 5)	0.339	260	1135	0.00
(6, 6)	0.407	312	1121	3.86
(7, 7)	0.475	364	1111	5.43
(8, 8)	0.542	416	1097	7.71
(9, 9)	0.610	468	1243	11.71
(10, 10)	0.678	520	1227	15.29
(11, 11)	0.746	572	1209	21.29
(12, 12)	0.814	624	1208	27.00
(13, 13)	0.881	676	1305	32.71
(14, 14)	0.949	728	1292	40.14
(15, 15)	1.017	780	1274	48.86
(16, 16)	1.085	832	1261	55.43

Results and discussion

The simulation trajectories show that the NM molecules cannot spontaneously enter the interior of (5,5) SWNT, which is coincident with the previous result of quantum mechanics study, i.e., the encapsulation of NM inside a (5,5) SWNT is an endothermic process [22]. Therefore, the simulation results for the SWNTs with larger radius are discussed as follows.

Structure Snapshots of confined NM inside the tubular cavities obtained from the simulation trajectories are displayed in Fig. 2. It is evident from the results that the confined NM molecules are arranged into an ordered fashion induced by the

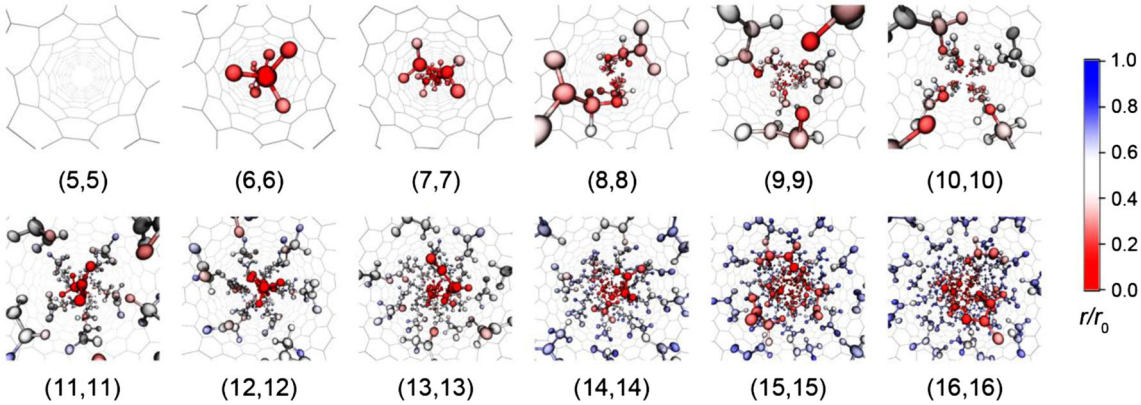

Fig. 2 Snapshots of the NM molecules confined in various SWNTs. Each atom of confined NM is colored according to the perpendicular distance from its centroid to the SWNT axis

tubular cavities. The linear structures near the tubular axis are found in both the (6,6) and (7,7) SWNTs while the double helix and triple helix structures are formed inside the (8,8) and (9,9) SWNTs, respectively. Furthermore, a quadrangular structure is observed in the (10,10) SWNT. As the SWNT radius increases, two-layer structures of the confined NM molecules appear. For the (11,11) and (12,12) SWNTs, the linear structures of NM are found in the inner layer while the pentagonal and hexagonal structures are formed in the outer layer, respectively. For the (13,13) SWNT, there exists an approximate linear structure in the inner layer and a blurry hepta helix in the outer layer. For the other larger SWNTs, the structural arrangement of two layers is still maintained. However, the structure of confined NM becomes less ordered both in the inner and outer layer. It can be inferred that there will exist a critical SWNT as the radius further increases where the structure of confined NM is almost the same as that of bulk NM. In short, the ordered and layered structures of NM molecules can be formed when confined in the tubular cavity, which is greatly dependent on the SWNT radius.

The transform of some molecular conformations resulting from the rotation of chemical bonds can be hindered inside the interior of nantoubes. For example, ethanol has two conformations, i.e., *gauche* and *trans* type. The previous MD simulation [39] has found that the percentage of *gauche* ethanol inside a (8,8) SWNT is higher than that of bulk ethanol. In contrast, this percentage inside a (6,6) SWNT is almost the same as that of bulk ethanol. Accordingly, the conformation transform between *eclipsed* and *staggered* NM at the confinement of SWNTs was analyzed on the basis of the distribution of CH_3–NO_2 dihedrals (see Fig. S1). The result shows that a uniform dihedral distribution ranging from −180° to 180° is observed in all the systems no matter whether there exists a nanotube or not, indicating that the influence of the SWNT confinement on the conformation transform between *eclipsed* and *staggered* NM is ignorable. The basic reason is that the NO_2 group can rotate around the C-N bond almost freely due to very low transform energy barrier.

Density On the basis of the average number of NM molecules confined in the SWTNs (see Table 1), the overall mass density of confined NM was calculated using the mass divided by the volume. Herein, two mass densities denoted by ρ and ρ′ are defined according to different volumes. In the former definition, the geometrical volume of SWNTs is employed where the carbon atoms of nanotubes are only regarded as the mass points. In the latter definition, the effective tubular volume is used where the intrinsic volume of SWNT atom is taken into account. Hence, the van der Waals radius of carbon atom, i.e., 0.1992 nm taken from CHARMM27 force filed [31], is simply subtracted from the SWNT radius. The mass density profiles of confined NM as a function of the SWNT radius are depicted in Fig. 3. It can be

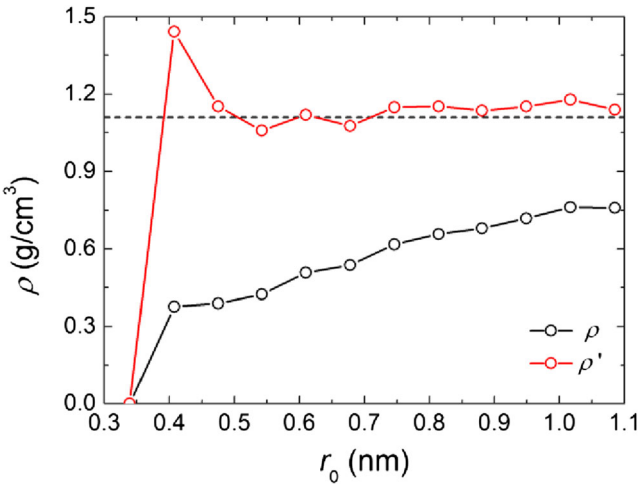

Fig. 3 The average mass density of confined NM as a function of the SWNT radius, ρ is calculated using the geometrical volume of SWNTs and ρ′ is calculated based on the effective volume of SWNTs where the van der Waals radius of carbon atoms is considered. The dash line is the average mass density of bulk NM.

seen clearly that ρ increases gradually as the SWNT radius increases, whereas it is still much less than the density of bulk NM. In sharp contrast, ρ′ fluctuates around the bulk NM density in all the SWNTs except (6,6) SWNT, meaning that the NM molecules can adopt suitable arrangement and orientation in the course of spontaneous entrance and the real volume occupied by confined NM is almost the same as that of bulk NM. For the high density of ρ′ inside the (6,6) SWNT, it is reasonable that the NM molecules need to be compressed slightly to enter into the extremely narrow cavity driven by strong van der Waals attractions.

Although ρ′ is nearly the same for all the nanotubes except the (6,6) SWNT, the local mass density may be different owing to the ordered structure of NM at the tubular confinement. Previous simulations have reported that the SWNT confinements on water can lead to higher local mass density than bulk density. To delve into the local mass density, the density distribution of confined NM along the radial direction of SWNT was calculated (see Fig. 4). It is noteworthy that the entire NM molecule is treated as a mass point and the radial distance is normalized by the SWNT radius for computation and comparison conveniences.

Not surprisingly, the radial mass densities are only located in certain regions. For example, rare high mass densities are found near the SWNT axis both in the (6,6) and (7,7) SWNTs. By contrast, the peaks of local mass density shift toward the nanotube wall for the (8,8), (9,9), and (10,10) SWNTs. This is because the NM molecules lying at the axis of narrow (6,6) and (7,7) SWNT can adequately interact with all the carbon atoms of SWNT to maximize the van der Waals interactions. As the SWNT radius increases, the van der Waals attractions between the confined NM and all the SWNT atoms become weak and cannot make the NM molecules stay near the SWNT axis. Hence, the NM molecules move close to the SWNT wall and are favored by the van der Waals attractions with the adjacent carbon atoms of SWNT.

For the (11,11) SWNT, the distribution of mass density begins to split into two peaks, which is in accord with the layered structure of confined NM (see Fig. 2). Inside the (11,11) and (12,12) SWNTs, the mass density of inner layer is higher than that of outer layer as a result of the linear structure at the SWNT axis. From the (11,11) to (16,16) SWNT, the mass density of inner layer decreases by degrees while the mass density of outer layer is almost constant. Besides, the peak of density distribution of inner layer shifts away from the SWNT axis and the corresponding shape becomes wide. It is reasonable that the NM molecules of outer layer directly interact with the SWNT wall through the van der Waals interactions, and thus can form more ordered structure than the inner layer NM. The structure of inner layer NM is

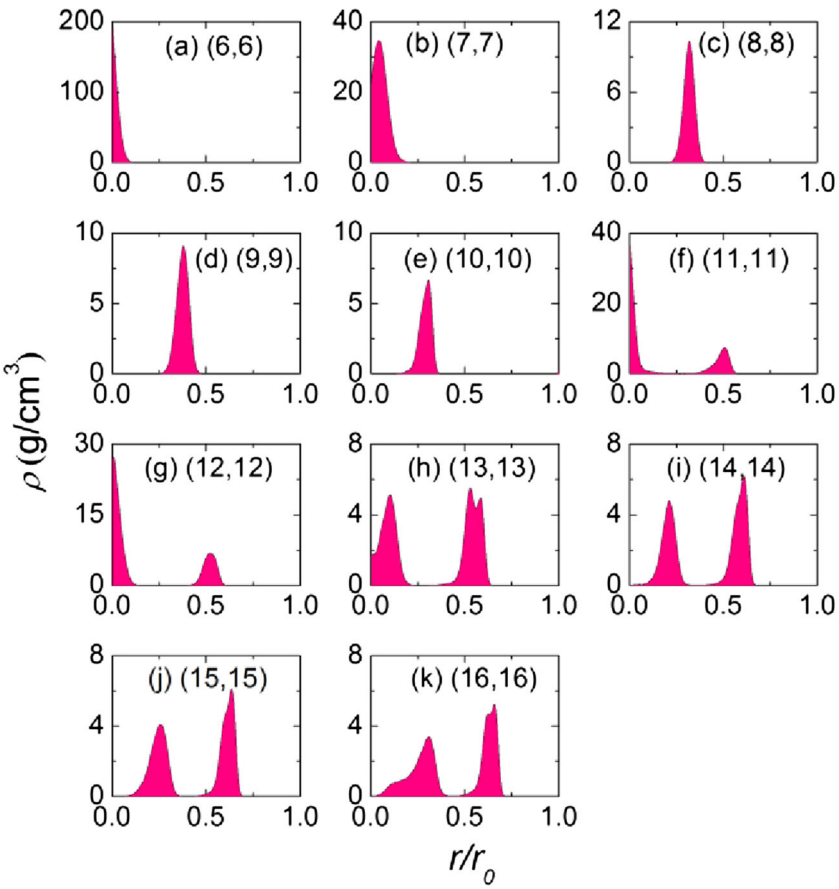

Fig. 4 Radial mass density profiles of the NM molecules confined in a series of SWNTs, r is the perpendicular distance from the NM centroid to the tubular axis and r_0 is the SWNT radius

mainly dominated by the outer layer NM through the complex intermolecular interactions, such as the van der Waals attractions and electrostatic interactions. Therefore, it can be concluded that the density of inner layer will continuously decrease and the corresponding structure will become less ordered as the SWNT radius further increases.

In addition, to further understand the three-dimensional mass density distribution of confined NM in various SWNTs, the spatial mass density distribution was calculated, which can provide a clear picture of the three-dimensional neighborhood surrounding a nanotube [40]. As delineated in Fig. 5, the ring-like distribution is observed outside the nanotube in all the systems, which is irrelevant of the SWNT radius. By comparison, both the shape and size of distribution inside the nanotube are greatly dependent on the SWNT radius. As the SWNT radius increases, the distribution shape gradually changes from one point, one ring, one ring surrounding one point, to two concentric rings. Moreover, the ring size also increases as a function of the SWNT radius. Obviously, these distinct distributions can be attributed to the ordered structural arrangement of confined NM in the tubular cavities.

Orientation At the nanoscale confinement, an obvious feature of molecules is the preferred orientation of certain chemical bonds and molecular dipole moments. On account of the molecular symmetry of NM, the dipole vector has the same direction as the N–C bond vector. Here, the orientation angle θ is defined as the angle between the molecular dipole vector of NM and the z axis, i.e., the SWNT axis. The cosine of θ was measured to describe the orientation of both molecular dipole and local N–C bond of confined NM. Furthermore, the orientation is closely related to the ordered structure of confined NM. The more concentrated the distribution of cosθ, the more ordered the corresponding structure.

The cosθ distributions of both confined and bulk NM were computed for comparison. As displayed in Fig. 6, a uniform distribution of bulk NM ranging from −1 to 1 is found, indicative of no preferred orientation. In contrast, the preferred orientation is observed for confined NM. For the (6,6), (10,10), (13,13), and (15,15) SWNTs, there exists only one peak gathered at the value of about −1 or 1, suggesting that the NM dipole prefers to lie parallel along the SWNT axis with one direction. The highest percentage is found in the (6,6) SWNT. For the (8,8), (9,9), (11,11), (12,12), and (14,14) SWNTs, there are two peaks located at the value of both about −1 and 1, indicative of the preferred parallel orientation of NM dipole with two opposite directions. Although two peaks is also found in the (16,16) SWNT, their percentages are low and all the orientation is covered, suggestive of a less ordered structure. More interestingly, a special distribution located around 0 is observed only in the (7,7) SWNT, revealing that the dipole orientation perpendicular to the SWNT axis is preferred. In short, there exist two preferred orientations of NM dipole at the tubular confinement, i.e., the perpendicular orientation in the (7,7) SWNT and the parallel orientation in the other SWNTs.

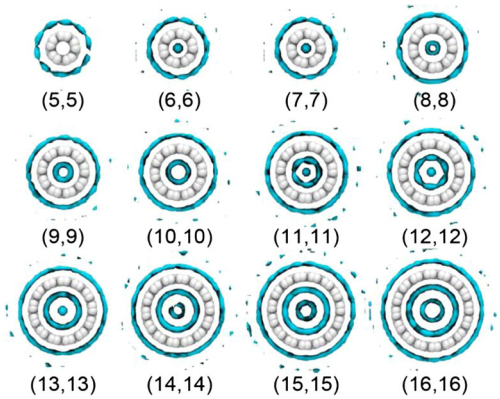

Fig. 5 Spatial mass density distribution of the NM molecules around a series of SWNTs, the surface shown corresponds to the isovaule of about 0.9

To further interpret the dipole orientation, the dipole vectors of confined NM were delineated for the final structure obtained from MD trajectory. It can be seen clearly from Fig. 7 that the arrangement of NM dipole vectors at the SWNT confinement is in a regular pattern. For instance, the dipole vectors are linked into a line end-to-end inside the (6,6) SWNT driven by the dipole-dipole interactions. For the special (7,7) SWNT, the dipole vectors point "up" and "down" along the tubular axis in turn, which may result from the balance of the dipole-dipole interactions of NM and the van der Waals attractions between NM and SWNT. From the (8,8) to (12,12) SWNT, the dipole vectors still align end-to-end in each queue. However, there exist two opposite dipole orientations in some SWNTs, which are colored in pink and cyan in Fig. 7. This phenomenon may be caused by the initial orientation of NM when spontaneously entering into the SWNT cavity. From the (13,13) to (16,16) SWNT, the orientations of dipole vectors become less ordered. This is because the effect of van der Waals interactions on the NM structure is weakened as the SWNT radius increases. From the above discussion, it can be deduced that the structural arrangements of confined NM are mainly governed by the van der Waals attractions of SWNT with NM and the corresponding preferred orientations are determined by the dipole-dipole interactions of NM.

Conclusions

A series of atomistic MD simulations have been performed to investigate the structural characteristics of liquid nitromethane confined inside the SWNT cavities. The ordered structures

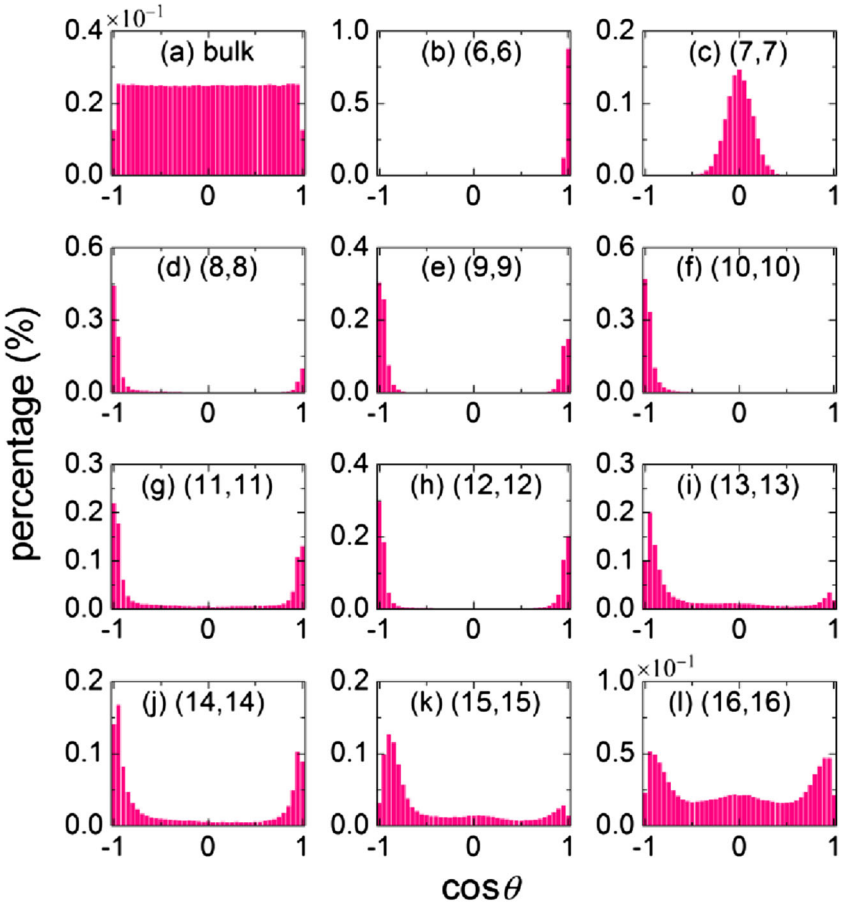

Fig. 6 Distributions of cosθ in various SWNTs calculated from the simulation trajectory of the last 5 ns, the orientation angle θ is defined as the angle formed between the NM dipole vector and z axis

with preferred orientations of confined NM were obtained arising from the van der Waals attractions of NM with SWNT and the dipole-dipole interactions of NM, which are greatly dependent on the SWNT radius. For example, a linear structure with the end-to-end alignment of dipole vectors parallel along the SWNT axis is formed in the (6,6) SWNT. By contrast, the side-by-side staggered arrangement of dipole vectors perpendicular to the SWNT axis is only found in the (7,7) SWNT. As the SWNT radius increases, two layered structures are observed beginning from the (11,11) SWNT, and the van der Waals interactions between the inner-layer NM and SWNT are weakened gradually, leading to less ordered structural arrangements and dipole orientations. In addition, the overall mass density of confined NM is basically the same as that of bulk NM while the local mass density is higher than that of bulk NM. Among all the SWNTs, the highest local mass density is gained in the (6,6) SWNT. On the basis of the results reported herein, the diffusion process and decomposition reactions of NM at the SWNT confinement should be explored in the future, which can further improve the understanding of the energy storage, controlled thermal decomposition pathway, and energy release of energetic molecules.

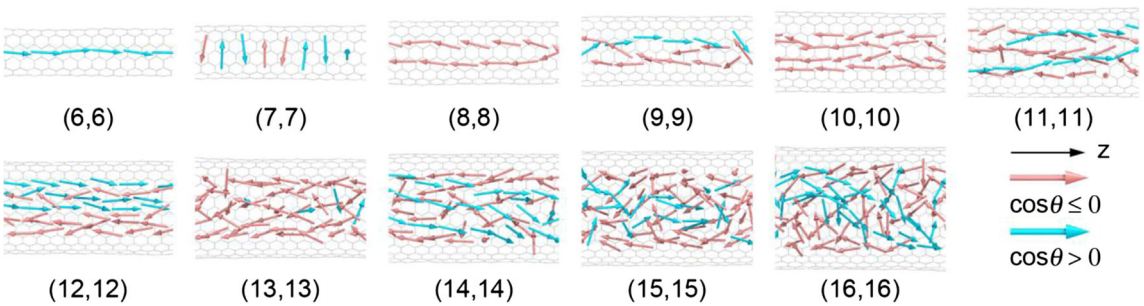

Fig. 7 Final snapshots of NM dipole vectors at the tubular confinement, θ is the orientation angle formed between the NM dipole vector and z axis. The dipole vector is colored in pink when the cosθ is less than or equal to 0, or cyan when the cosθ is more than 0

Acknowledgments This study was supported by the National Natural Science Foundation of China (Nos. 21403162). Thu authors also thank Prof. Yuanjie Shu for his valuable comments and constructive suggestions on this paper.

References

1. Eremets MI, Gavriliuk AG, Trojan IA, Dzivenko DA, Boehler R (2004) Nat Mater 3:558–563
2. Christe KO (2007) Propellants, Explos, Pyrotech 32:194–204
3. Tasis D, Tagmatarchis N, Bianco A, Prato M (2006) Chem Rev 106: 1105–1136
4. Khlobystov AN, Britz DA, Briggs GAD (2005) Acc Chem Res 38: 901–909
5. Abou-Rachid H, Hu A, Timoshevskii V, Song Y, Lussier LS (2008) Phys Rev Lett 100:196401
6. Ji W, Timoshevskii V, Guo H, Abou-Rachid H, Lussier LS (2009) Appl Phys Lett 95:021904
7. Timoshevskii V, Ji W, Abou-Rachid H, Lussier LS, Guo H (2009) Phys Rev B 80:115409
8. Zheng FW, Yang Y, Zhang P (2012) Int J Mod Phys B 26:1250047
9. Sharma H, Garg I, Dharamvir K, Jindal VK (2010) J Phys Chem C 114:9153–9160
10. Smeu M, Zahid F, Ji W, Guo H, Jaidann M, Abou-Rachid H (2011) J Phys Chem C 115:10985–10989
11. Alper HE, Abu-Awwad F, Politzer P (1999) J Phys Chem B 103: 9738–9742
12. Sorescu DC, Rice BM, Thompson DL (2000) J Phys Chem B 104: 8406–8419
13. Sorescu DC, Rice BM, Thompson DL (2001) J Phys Chem A 105: 9336–9346
14. Alavi S, Thompson DL (2004) J Chem Phys 120:10231–10239
15. Kabadi VN, Rice BM (2004) J Phys Chem A 108:532–540
16. Megyes T, Bálint S, Grósz T, Radnai T, Bakó I, Almásy L (2007) J Chem Phys 126:164507
17. Appalakondaiah S, Vaitheeswaran G, Lebègue S (2013) J Chem Phys 138:184705
18. Siavosh-Haghighi A, Thompson DL (2006) J Chem Phys 125: 184711
19. Siavosh-Haghighi A, Sewell TD, Thompson DL (2010) J Chem Phys 133:194501
20. Xu JC, Zhao JJ (2009) Acta Phys Sin 58:4144–4149
21. Chang J, Lian P, Wei DQ, Chen XR, Zhang QM, Gong ZZ (2010) Phys Rev Lett 105:188302
22. Wang LX, Yi CH, Zou HT, Xu J, Wu WL (2010) Chem Phys 367: 120–126
23. Han SP, van Duin ACT, Goddard WA, Strachan A (2011) J Phys Chem B 115:6534–6540
24. Rom N, Zybin SV, van Duin ACT, Goddard WA, Zeiri Y, Katz G, Kosloff R (2011) J Phys Chem A 115:10181–10202
25. Guo F, Cheng XL, Zhang H (2012) J Phys Chem A 116: 3514–3520
26. Liu LM, Car R, Selloni A, Dabbs DM, Aksay IA, Yetter RA (2012) J Am Chem Soc 134:19011–19016
27. Zhang L, Chen L (2013) Acta Phys Sin 62:138201
28. Lide DR (2004) CRC handbook of chemistry and physics, 84th edn. CRC, Boca Raton
29. Alexiadis A, Kassions S (2008) Chem Rev 108:5014–5034
30. Vanommeslaeghe K, Hatcher E, Acharya C, Kundu S, Zhong S, Shim J, Darian E, Guvench O, Lopes P, Vorobyov I, Mackerell AD (2010) J Comput Chem 31:671–690
31. MacKerell AD, Bashford D, Bellott M, Dunbrack RL, Evanseck JD, Field MJ, Fischer S, Gao J, Guo H, Ha S, Joseph-McCarthy D, Kuchnir L, Kuczera K, Lau FTK, Mattos C, Michnick S, Ngo T, Nguyen DT, Prodhom B, Reiher WE, Roux B, Schlenkrich M, Smith JC, Stote R, Straub J, Watanabe M, Wiorkiewicz-Kuczera J, Yin D, Karplus M (1998) J Phys Chem B 102:3586–3616
32. Phillips JC, Braun R, Wang W, Gumbart J, Tajkhorshid E, Villa E, Chipot C, Skeel RD, Kale L, Schulten K (2005) J Comput Chem 26: 1781–1802
33. Feller SE, Zhang Y, Pastor RW, Brooks BR (1995) J Chem Phys 103: 4613–4621
34. Tuckerman M, Berne BJ, Martyna GJ (1992) J Chem Phys 97:1990–2001
35. Ryckaert JP, Ciccotti G, Berendsen HJC (1977) J Comput Phys 23: 327–341
36. Andersen HC (1983) J Comput Phys 52:24–34
37. Darden T, York D, Pedersen L (1993) J Chem Phys 98: 10089–10092
38. Humphrey W, Dalke A, Schulten K (1996) J Mol Graph 14: 33–38
39. Shao Q, Huang LL, Zhou J, Lu LH, Zhang LZ, Lu XH, Jiang SY, Gubbins KE, Zhu YD, Shen WF (2007) J Phys Chem C 111:15677–15685
40. Balamurugan K, Baskar P, Kumar RM, Das S, Subramanian V (2012) J Phys Chem C 116:4365–4373